Supporting Information

Bypassing the Scaling Relationship with Spin Selectivity: Construction of Lewis Base Functionalized Hetero-Structural 2D Nanosheets for Enhanced Oxygen Evolution Reaction

Arun Karmakar,[†‡] Durairaj Mahendiran,[†#] Ragunath Madhu,[†‡] Palanichamy Murugan,[†#*] and Subrata Kundu [†‡*]

[†]*Academy of Scientific and Innovative Research (AcSIR), Ghaziabad-201002, India.*

[‡]*Electrochemical Process Engineering (EPE) Division, CSIR-Central Electrochemical Research Institute (CECRI), Karaikudi-630003, Tamil Nadu, India.*

[#]*Electrochemical Power Sources (ECPS) Division, CSIR-Central Electrochemical Research Institute (CECRI), Karaikudi-630003, Tamil Nadu, India.*

*To whom correspondence should be addressed, *E-mail:* murugan@cecri.res.in *and* skundu@cecri.res.in*;* Phone/Fax: (+ 91) 4565-241487.

This file contains 29 pages in which the details of Electrodes fabrications, material preparation for different characterizations, data for OER, comparative electrocatalysis datas are given in detail.

Number of Figure: 17

Number of Table: 2

1. Reagents and Instruments:

Cobalt Nitrate [$Co(NO_3).6H_2O$], Iron Nitrate [$Fe(NO_3)_3.9H_2O$], Nickel Nitrate [$Ni(NO_3).6H_2O$], Thiourea and ammonium fluoride (NH_4F) were were purchased from Sigma-Aldrich and used as received. Sodium carbonate (Na_2CO_3) was purchased from Merck and used as received. The used carbon cloth as working electrode substrate purchased from Sigma-Aldrich and used after surface cleaning. DI water was used throughout entire experiments. ICP-MS analysis was carried by using iCAP RQ from thermoscientific instrument. The as prepared catalysts with different stoichiometric ratios were characterized with HR-TEM, (Tecnai^{TM} G^2 TF20) working at an accelerating voltage of 200 kV and by Talos F-200-S with HAADF elemental mapping. Energy Dispersive X-ray Spectroscopy (EDS) analysis were carried out with the FE-SEM instrument with the images (SUPRA 55VP Carl Zeiss). Scanning Electron Microscopy (SEM) analysis was carried with a Hitachi, Japan make model S-3000H instrument having magnification 30X to 300 KX with the accelerating voltage ~ 0.3 to 30 kV. The XRD analysis carried out with a scanning rate of 5° min^{-1} in the 2θ range 10-90° using a Rigaku X-ray powder diffractometer (XRD) with Cu K_α radiation (λ = 0.154 nm). X-ray photoelectron spectroscopic (XPS) analysis was performed using a Theta Probe AR-XPS system (Thermo Fisher Scientific, UK).

2. Electrochemical Characterization:

The electrochemical analyzer AURT-M204 has utilized for all electrochemical characterizations. The used Hg/HgO (1 M KOH) electrode used as reference electrode was purchased from CH instrument. The graphite rod was purchased from Alfa Aesar and has used as the counter electrode. Entire potential data that were collected by taking Hg/HgO as a reference electrode and later it was converted to reversal hydrogen electrode (E_{RHE}) scale by considering the Nernst equation of

$$E_{RHE} = E_{ref} + 0.059\times14 + 0.098 \quad \text{S1}$$

Over potential (η) values of bare CoFe-LDH, Ni_3S_4@CoFe-LDH, Ni_3S_4 and other catalyst at benchmarking current density of 10 mA/cm^2 is calculated by following this equation

$$\eta = E_{RHE} - 1.23\ V \quad \text{S2}$$

Tafel slope was calculated from 100 % iR-corrected LSV polarization data followed by fitting η *vs* log(j) using the Tafel equation

$$\eta = \beta \cdot \log(j/j_0) \quad \text{S3}$$

where β represents the Tafel slope, j signifies the current density and j_0 is the exchange current density. Electrochemical impedance spectroscopy (EIS) measurements were done on the frequency ranges from 10^5 to 1 Hz at 300 mV *vs* RHE. In addition, the Operando-EIS study has done by using modified GC electrode as working electrode at different applied potential. The value of electrochemical active surface areas (ECSA) can be measured by determining the electrochemical double layer capacitance (C_{dl}) as follows:

$$\Delta J = \nu \times C_{dl} \quad \text{Equation S4}$$

$$ECSA = \frac{C_{dl}}{C_s} \quad \text{Equation S5}$$

where ΔJ indicates the double-layer charging current resulting from scan-rates (ν) dependent CVs at non-faradic potential, C_s denotes a specific capacitance value of 0.040 mF/cm^2 depending on the typical reported values. The specific activity of the catalysts was determined by normalizing the geometrically normalized current density with respect to electrochemical active surface area (ECSA) values i.e.,

$$J_{ECSA} = \frac{J_{geo}}{ECSA} \quad \text{Equation S6}$$

All the electrodes have been fabricated by the conventional drop-casting method. Typically, the catalyst ink was prepared by taking 3 mg of catalyst powder in a solution mixture containing

750 µl of H_2O, 200 µl of ethanol, and 50 µl of 5% Nafion solution. Then 34.5 µl of catalyst ink was drop-casted over carbon with an effective surface area of 1×0.5 cm^2.

$$\text{Hence, loading is} = \frac{3 \times 34.5}{1000} \sim 0.1045 \text{ mg of catalyst} \ldots\ldots\ldots \text{ Equation S7}$$

The mass activity was calculated by employing the following relation at a particular overpotential value:

$$J_{mass} = \frac{J\ (mA)}{loading\ (mg)} \ldots\ldots\ldots \text{ Equation S8}$$

Electrochemical characterization in presence of external magnetic field has done by using Hall effect instrument of model no: DHE-21-C1.

3. Synthesis of pristine CoFe-LDH:

The pristine or Bare CoFe-LDH was prepared by following previous report with slight modification. Typically, 0.01 M of $Co(NO_3).6H_2O$ and 0.01 M of $Fe(NO_3)_3.9H_2O$ were added in 35 mL of DI water followed by stirring for 30 minutes to get clear solution. The resulted solution is coined as 'Solution A'. In another beaker contained 35 mL of DI water, 0.5 M of Na_2CO_3 were mixed thoroughly and stirred for 30 minutes. The resulted solution was named as 'Solution B' and later the same has transferred to a burette with volume capacitance of 50 mL. Later on, the 'Solution B' was added to 'Solution A' from the burette by fixing in such way that the flow rate become 10-15 drops/minute with a continuous stirring. The slow precipitation technique was followed to ensure the slow growth of LDH particles. Once, the entire carbonate solution added to the metal solution, the mixture was additionally stirred for 30 minutes. After completion of the reaction, the crude product was separated by centrifugation. At last, the brown color product was dried in hot air over for 12 hours at 60 ^oC.

4. Synthesis of Ni_3S_4@CoFe-LDH:

A simple one step solvothermal procedure was followed from growing Ni_3S_4 particle over CoFe-LDH. At first, 100 mg of CoFe-LDH powder was dispersed in 35 mL of N, N di-methyl formamide (DMF) by ultrasonication for 30 minutes. Next, 0.3 mM of $Ni(NO_3)_2.6H_2O$ and 0.4 mM of thiourea was added to the ultrasonicated solution. After adding the required salt and sulphide source the mixture was vigorously for 30 minutes. Once, complete homogeneity was achieved the solution was transferred Teflon-lined autoclave followed by solvothermal treatment at 180 ºC for 6 hours. Once, the solvothermal treatment has done the crude product wash collected via centrifugation followed by washing with water ethanol mixture. Pictorial representation of synthetic method has portrayed in Figure 1 of manuscript file. Pristine Ni_3S_4 was synthesized by following similar method except addition of CoFe-LDH powder.

5. Determination of Surface concentration of CoFe-LDH from the redox features of CV:

Calculated area associated with the oxidation of Co^{2+} to Co^{3+} = 0.000304 VA

Hence, the associated charge is = 0.000304 VA / 0.1 Vs^{-1}

= 0.00304 As

= 0.00304 C

Now, the number of electron transferred is = 0.00304 C / 1.602 $\times 10^{-19}$ C

= 1.89 $\times 10^{16}$ C

Since, the oxidation of Co^{2+} to Co^{3+} is a single electron transfer reaction, the number electron calculated above is exactly the same as the number of surface-active sites.

Hence, the number of Co participate in OER is = 1.89 $\times 10^{16}$ C

Determination of Turnover Frequency (TOF) from OER Current Density TOF in our study was calculated assuming that the surface-active Co atoms that had undergone the redox reaction just before onset of OER only participated in OER electrocatalysis. The corresponding expression is,

$$TOF = j \times N_A / F \times n \times \Gamma$$

Where, j = current density N_A= Avogadro number F = Faraday constant n = Number of electrons Γ = Surface concentration.

Hence, we have,

$TOF_{1.55\ V} = [(60\times 10^{-3})\ (6.023\times 10^{23})] / [(96485)\ (4)\ (1.89\times 10^{16})]$

$= 4.93\ sec^{-1}$

6. Magnetic measurement:

The temperature dependent magnetic results of both the pristine CoFe-LDH and Ni_3S_4@CoFe-LDH are given in Figure. The Currie constant (C) values for both the catalysts are calculated from the slope of χ_M vs (1/T) plot given in the Figure. The calculated C values for CoFe-LDH and Ni3S4@CoFe-LDH are 9.11 and 10.35 emu. K. g^{-1} respectively. The effective magnetic moment moments for both the catalyst are calculate by using the formula, $\mu_{eff} = 2.34\sqrt{C}$. The obtained magnetic moment values for CoFe-LDH and Ni_3S_4@CoFe-LDH are 7.06 and 7.6 μ_B respectively. The contribution of Co^{2+} and Fe^{3+} ions towards the net magnetic moment was calculated without considering any contribution from the nickel ions (owing to low concentration of Ni), by utilizing the equation, $\mu_{eff}^2 = \mu_{Fe+}^2\ \mu_{Co}^2$. From the XPS and DFT study we have seen that Ni_3S_4 does not effectively interact with the Fe^{3+} ions, so here we consider that the magnetic moment delivered by the high spin Fe^{3+} ions is constant in the both cases. Therefore, the change in magnetic moment value has arises from the Co^{2+} site as result of magnetic ordering by synergistic electron transfer to the sulphide lattice.

Total magnetic moment of Ni_3S_4@CoFe-LDH = 7.6 μ_B.

$$\mu_{Fe} = 2 \times \sqrt{\frac{5}{2}(\frac{5}{2}+1)}\ \mu_B = 5.47\ \mu_B.$$

Hence, $\mu_{Co} = (7.6 - 5.47)\ \mu_B = 2.13\ \mu_B$.

On the other hand, magnetic moment of CoFe-LDH = 7.06 μ_B. Therefore, μ_{Co} = (7.06 - 5.47) μ_B = 1.59 μ_B.

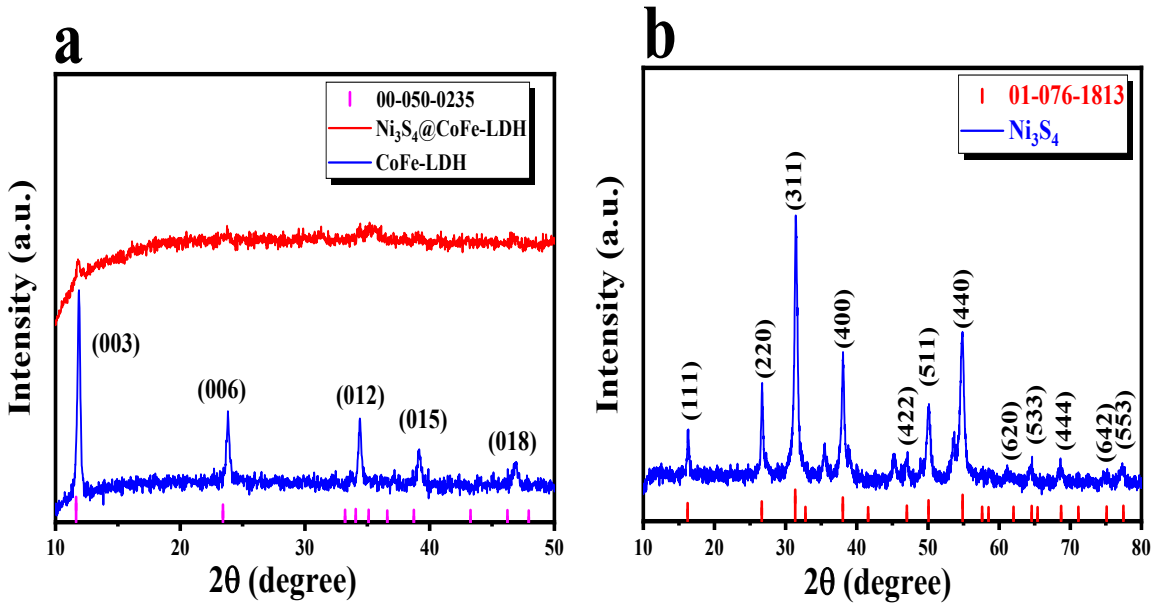

Figure S1: (a) X-ray diffraction pattern for pristine CoFe-LDH and Ni_3S_4@CoFe-LDH along with ICCD Card No: 00-050-0235 information and (b) X-ray diffraction pattern for pristine Ni_3S_4.

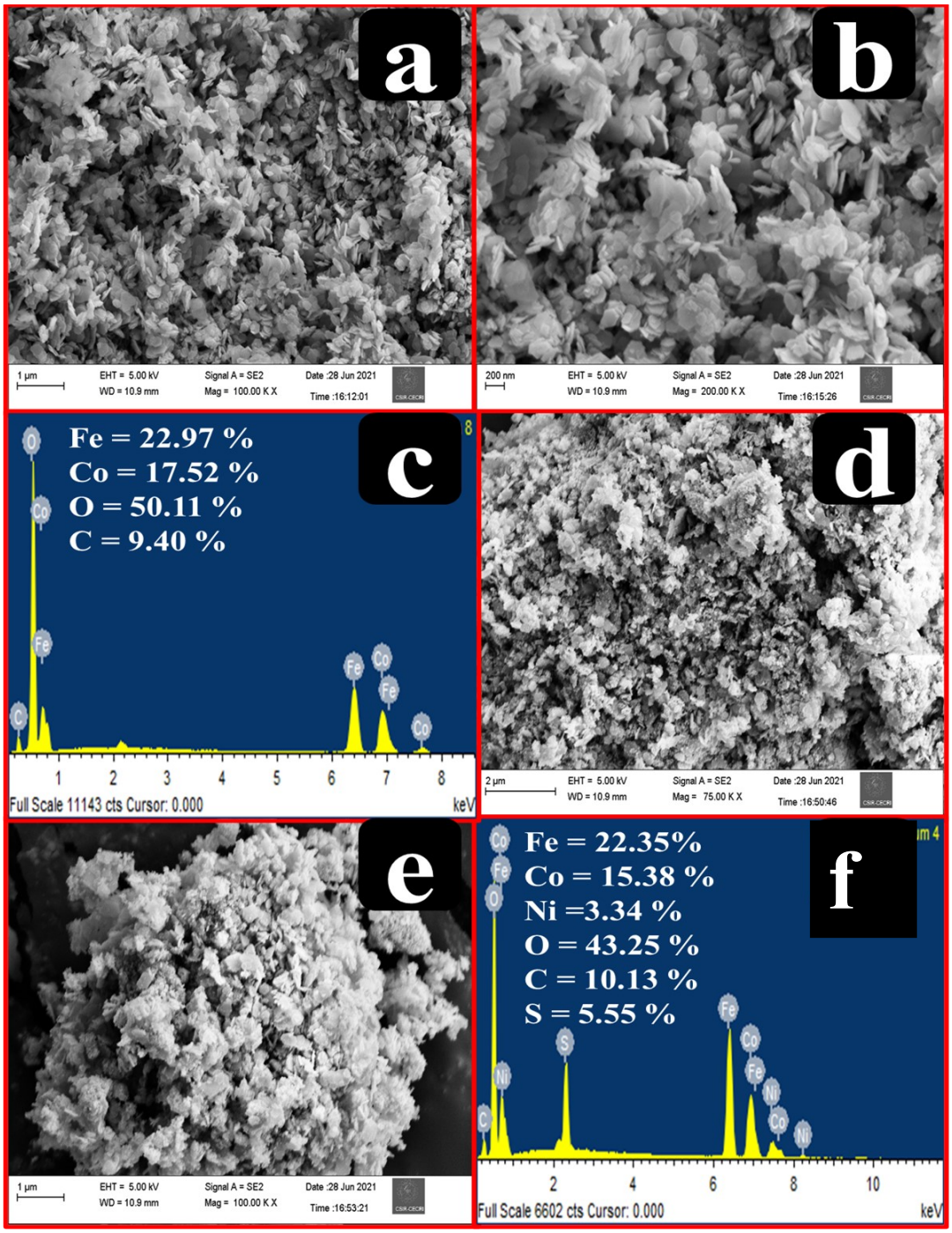

Figure S2: (a-b) low to high magnified FE-SEM images of pristine CoFe-LDH; (c) EDS spectrum of pristine CoFe-LDH with respective elemental signal and quantitative percentage; (d-e) low to high magnified FE-SEM images of Ni_3S_4@CoFe-LDH; (f) EDS spectrum of Ni_3S_4@CoFe-LDH with respective elemental signal and quantitative percentage.

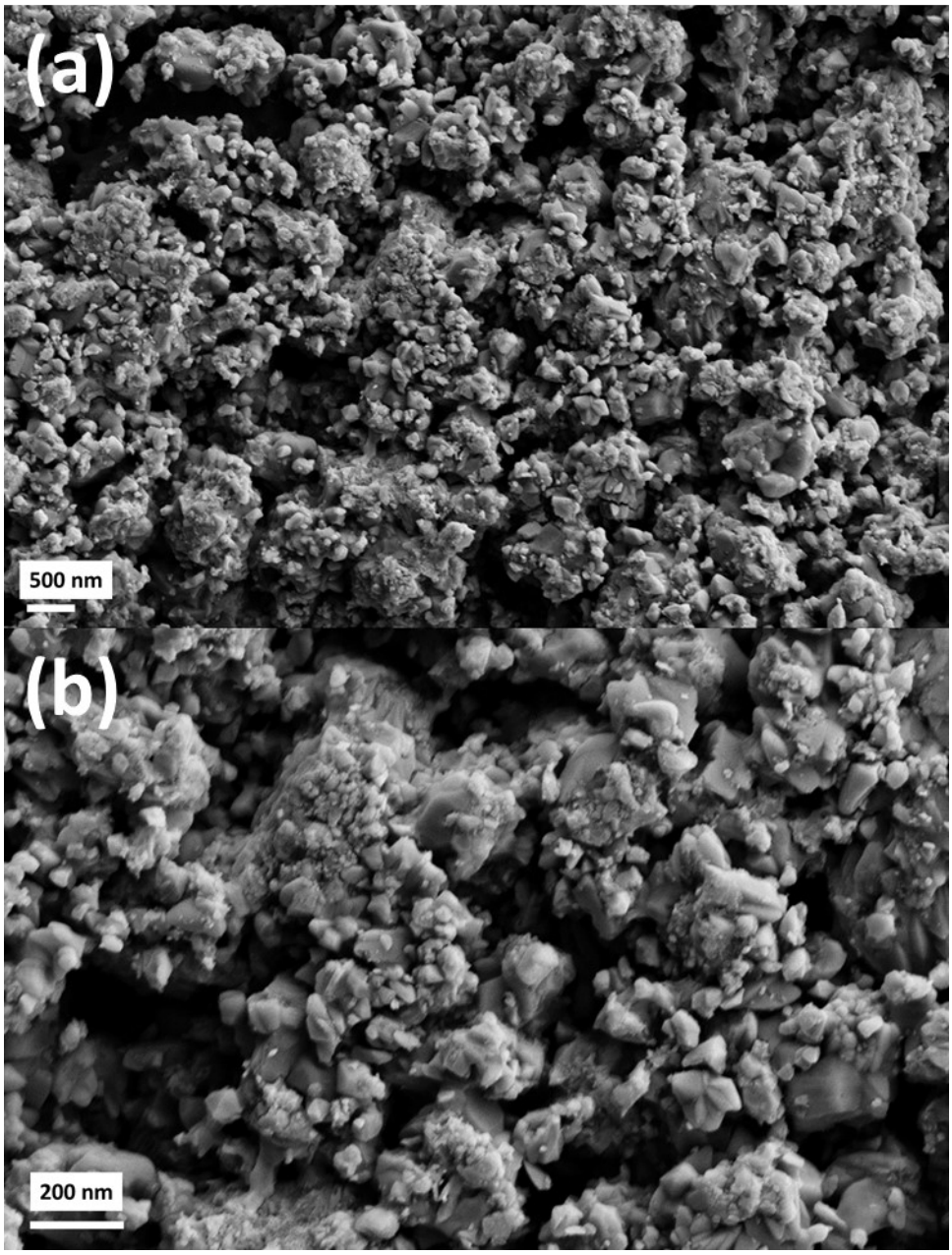

Figure S3: (a-b) low to high magnified SEM images for pristine Ni_3S_4 materials revealing undefined block like 3D particle structure.

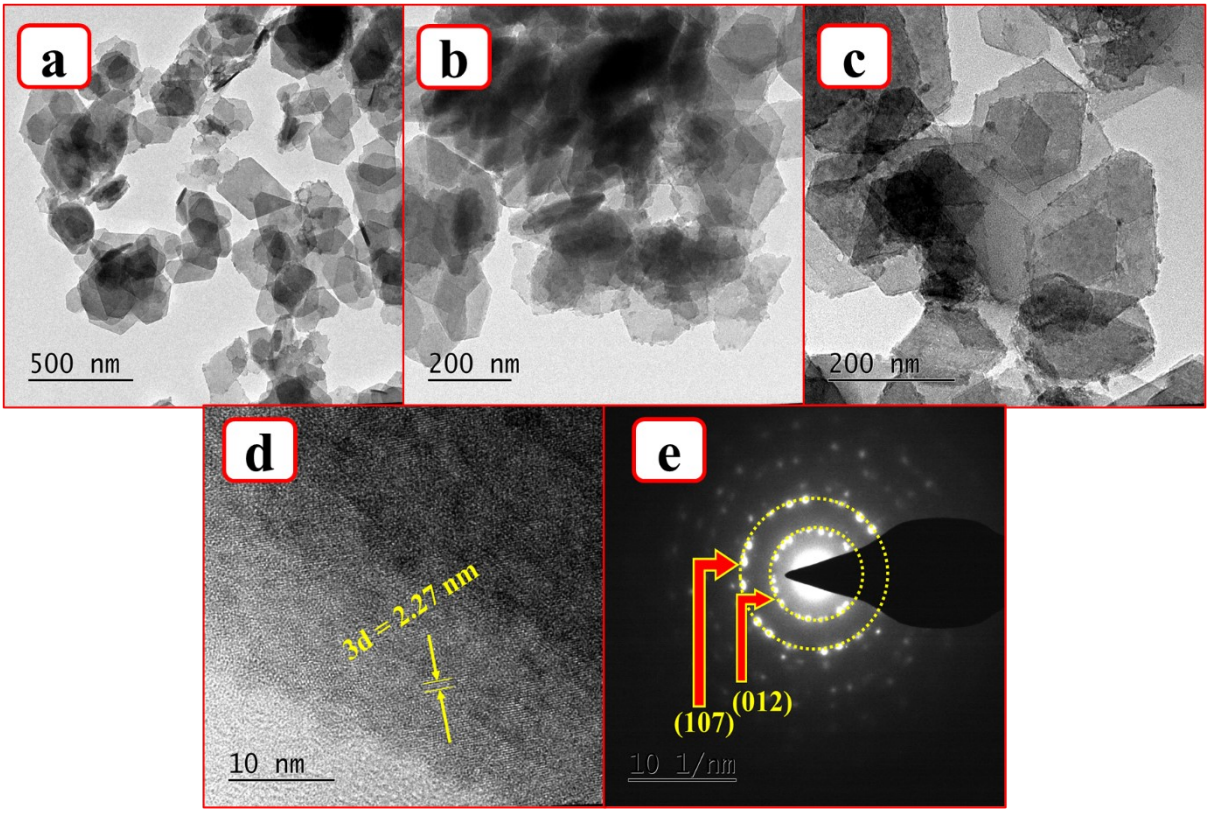

Figure S4: (a-c) low to high magnified TEM image of pristine CoFe-LDH which portrays the sheet like structure; (d) high resolution TEM image for lattice fringes analysis which shows the d-spacing value of 0.75 nm corresponding to the (003) planes of sheet like LDH structure and (d) selected area electron diffraction (SAED) pattern which portrays the diffraction pattern for (012) and (107) planes of (107) planes.

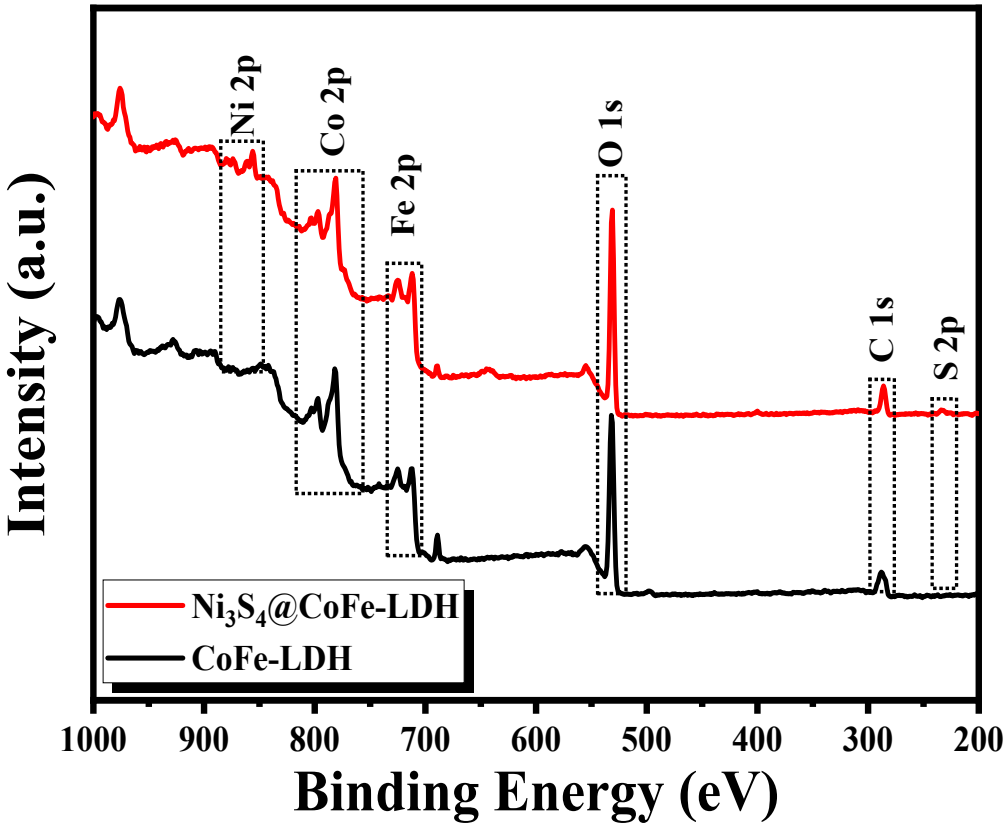
Intensity (a.u.)
Ni 2p
Co 2p
Fe 2p
O 1s
C 1s
S 2p
Ni3S4@CoFe-LDH
CoFe-LDH
1000
900
800
700
600
500
400
300
200
Binding Energy (eV)

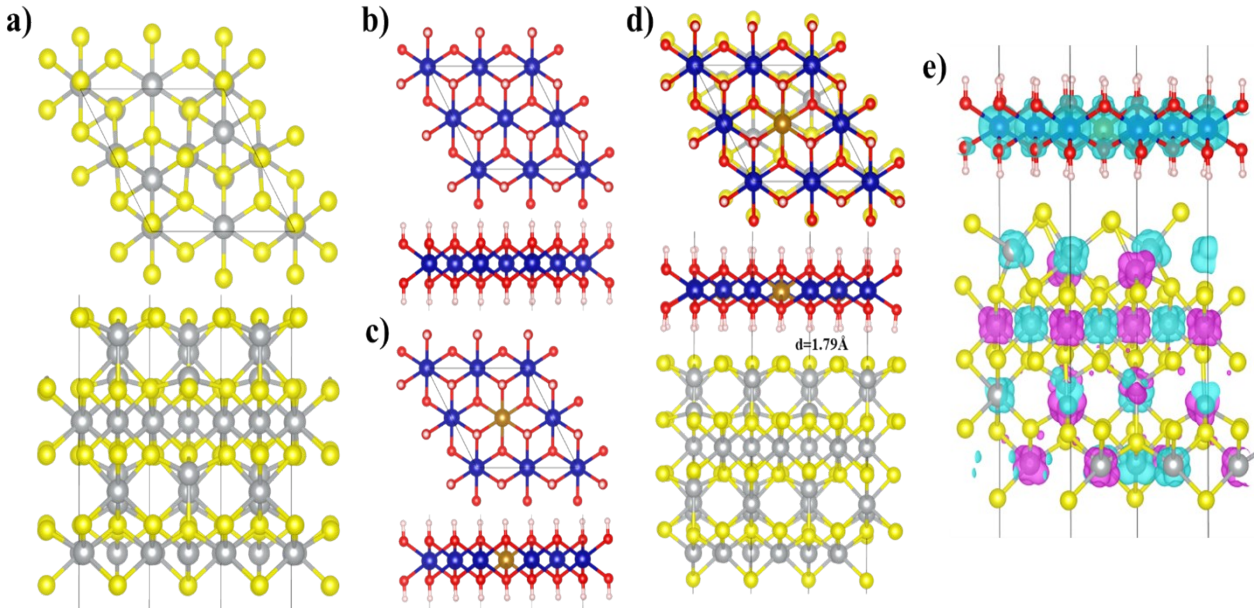

Figure S6: Ball-and-stick models illustrating the optimized structure of a) Ni_3S_4, b-c) pristine $Co(OH)_2$ without and with Fe doping, d) Top and side view of the CoFe-LDH/Ni_3S_4 heterostructure. In the figure, the following color scheme is used: yellow, grey, blue, brown, red, and pink balls represent sulfur, nickel, cobalt, iron, oxygen, and hydrogen atoms, respectively. e) The spin density plot of the CoFe-LDH/Ni_3S_4 heterostructure, where the cyan and pink colors indicate positive and negative spin of the system.

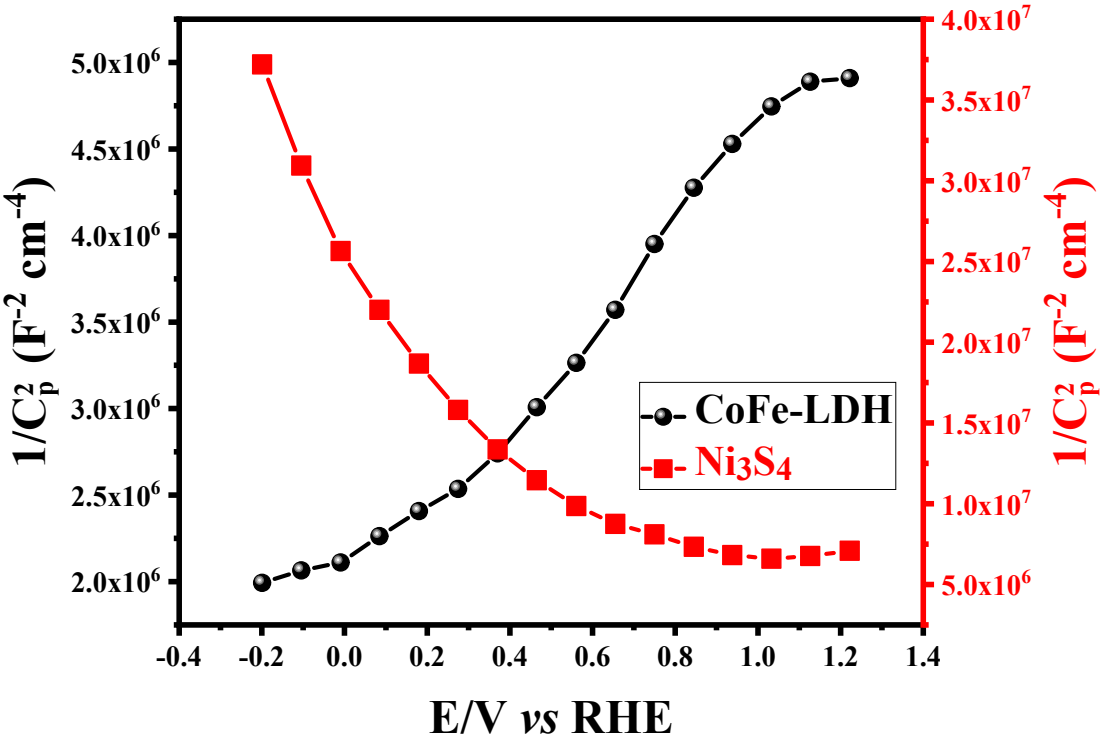

Figure S7: Mott-Schottky plot for Ni_3S_4 and CoFe-LDH obtained in the potential range of -0.2 to 1.25 V vs RHE.

System	E_b (eV)	M(μ_B)	a=b (Å)	Bond distances (Å)				d (Å)
				Co-O	Fe-Co	Fe-O	Ni-S	
$Co(OH)_2$	-	12.0	6.33	2.09	-	-	-	-
$Fe@Co(OH)_2$	-	13.0	6.33	2.12	3.17	2.13	-	-
Ni_3S_4	-	0.0	6.62	-	-	-	2.30	-
$Fe@Co(OH)_2/Ni_3S_4$	1.77	16.8	6.62	2.20	3.30	2.12	2.33	1.79

Table S1. Binding energy (E_b), total magnetic moments (M), Bond distances values along with interlayer distance (vertical distance) d values is also provided. The Binding energy formula, which can be expressed as : $E_b = -(E_{Fe@Co(OH)_2/Ni_3S_4} - E_{Fe@Co(OH)_2} - E_{Ni_3S_4})$.

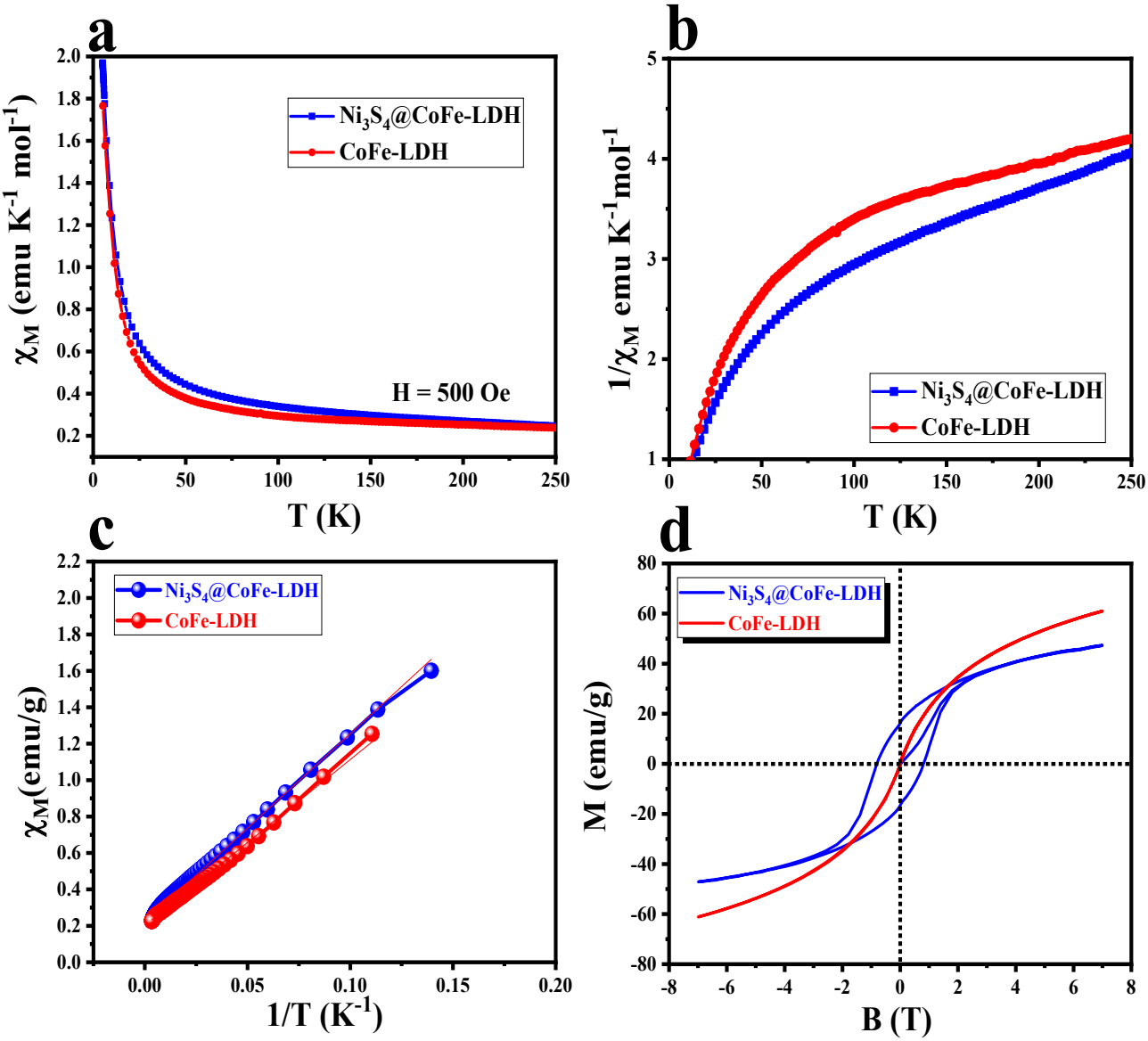

Figure S8. Magnetic properties of CoFe-LDH$_{0.5}$ and CoFe-LDH$_{1.5}$ (a) molar magnetic susceptibility (χ_M) vs Temperature (T) plot; (b) represent the temperature dependence of $1/\chi_M$ *vs* T plot; (c) fitted magnetic susceptibility data to the Curie-Weiss law χ_M vs $1/T$ plot to derive the Curie constant (C) values and (d) magnetic hysteresis curve.

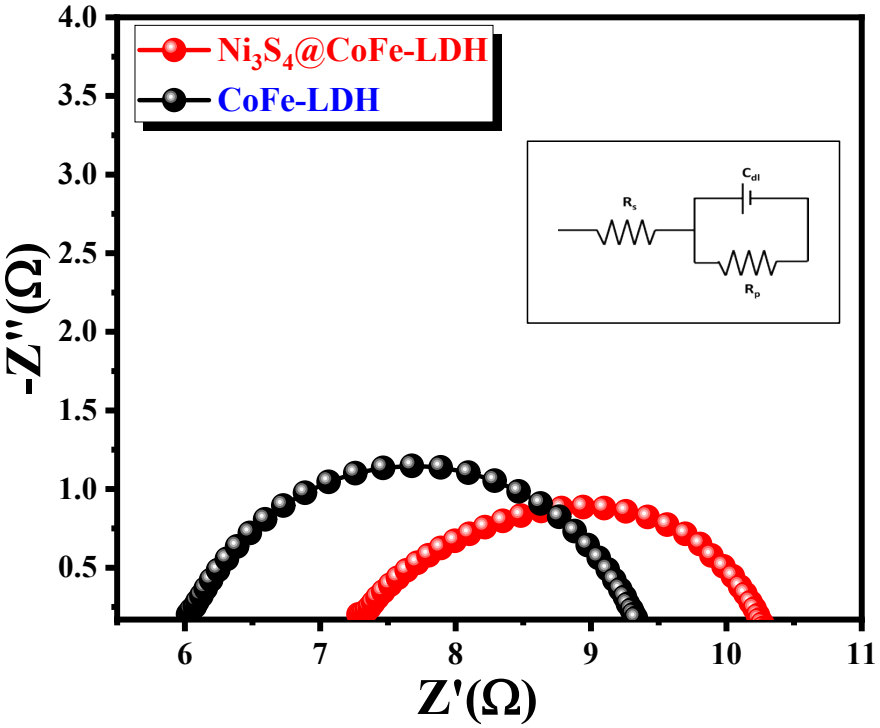
Ni3S4@CoFe-LDH
CoFe-LDH
Cdl
Rs
Rp
-Z''(Ω)
Z'(Ω)
4.0
3.5
3.0
2.5
2.0
1.5
1.0
0.5
6
7
8
9
10
11

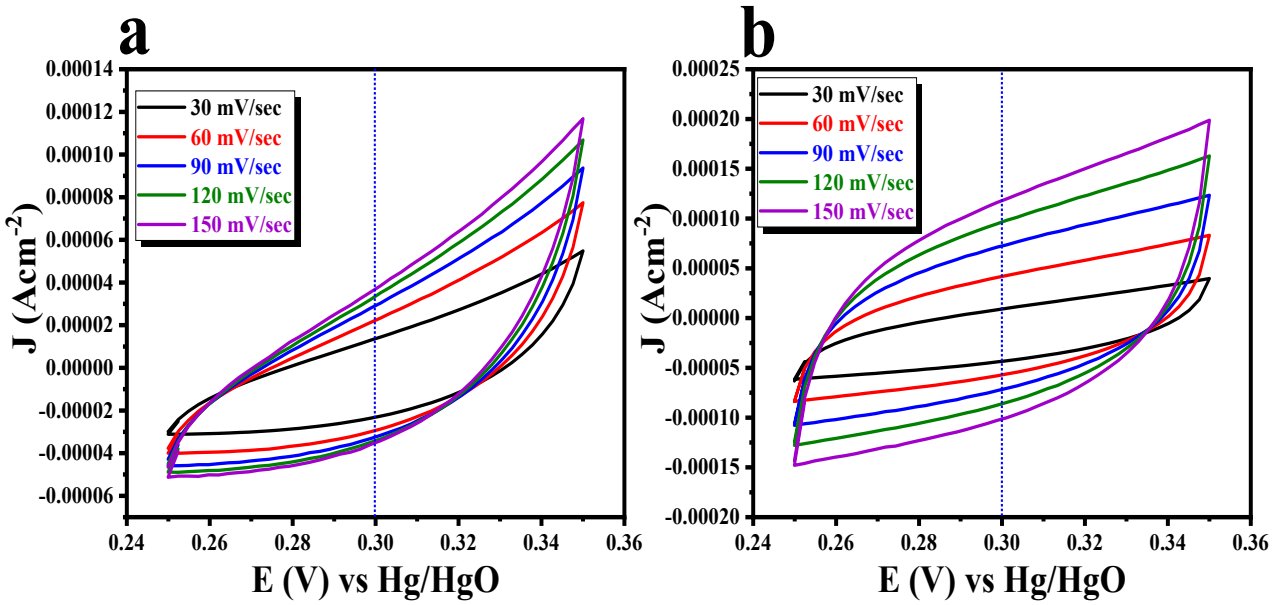

Figure S10. (a-b) Respective scan rate dependent CV features for pristine CoFe-LDH and Ni_3S_4@CoFe-LDH in non-faradaic region. The same has used to determine the double layer capacitance value of all the catalyst.

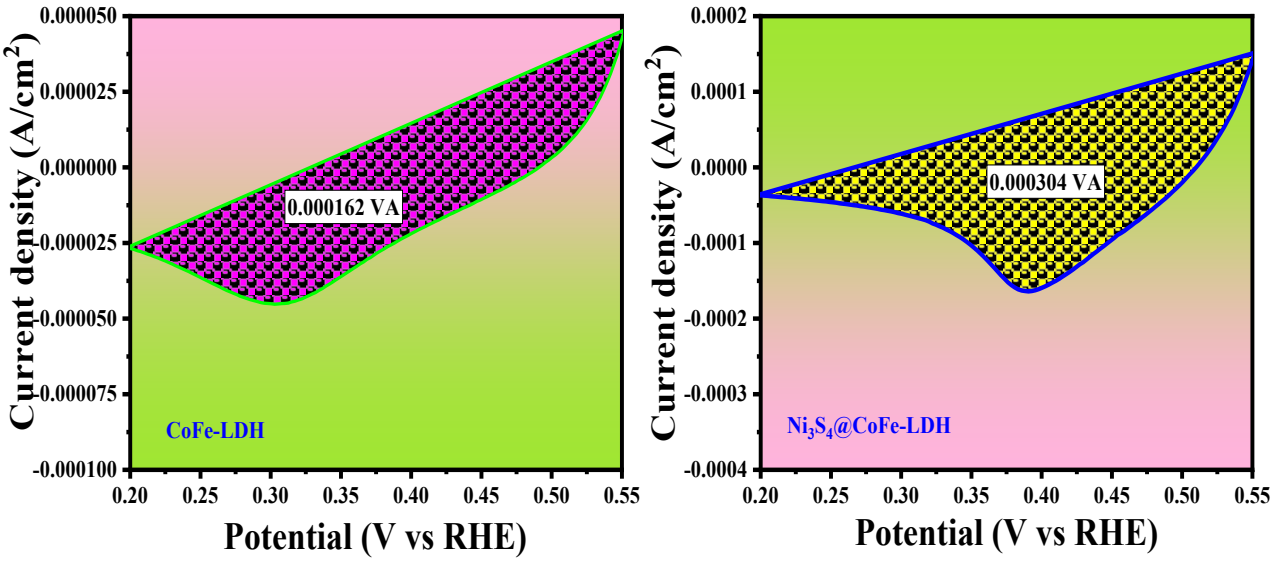

Figure S11. Reduction surface are of pristine CoFe-LDH and Ni_3S_4@CoFe-LDH.

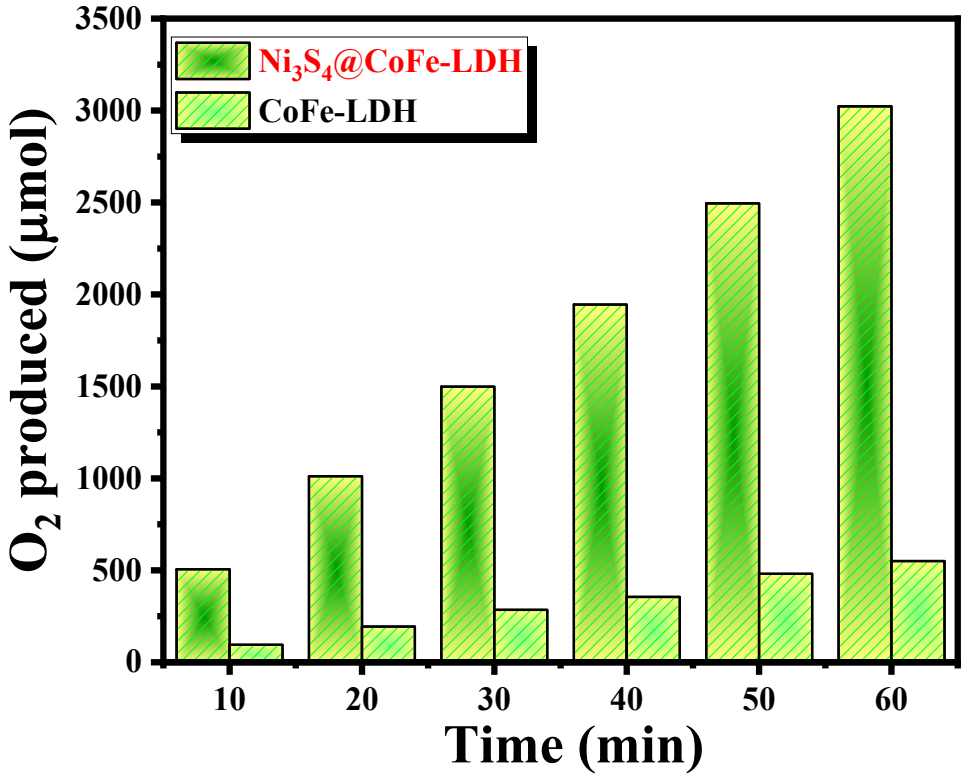

Figure S12. Quantitative analysis of produced O_2 in Ni_3S_4@CoFe-LDH and CoFe-LDH with different time interval measured via gas-chromatography.

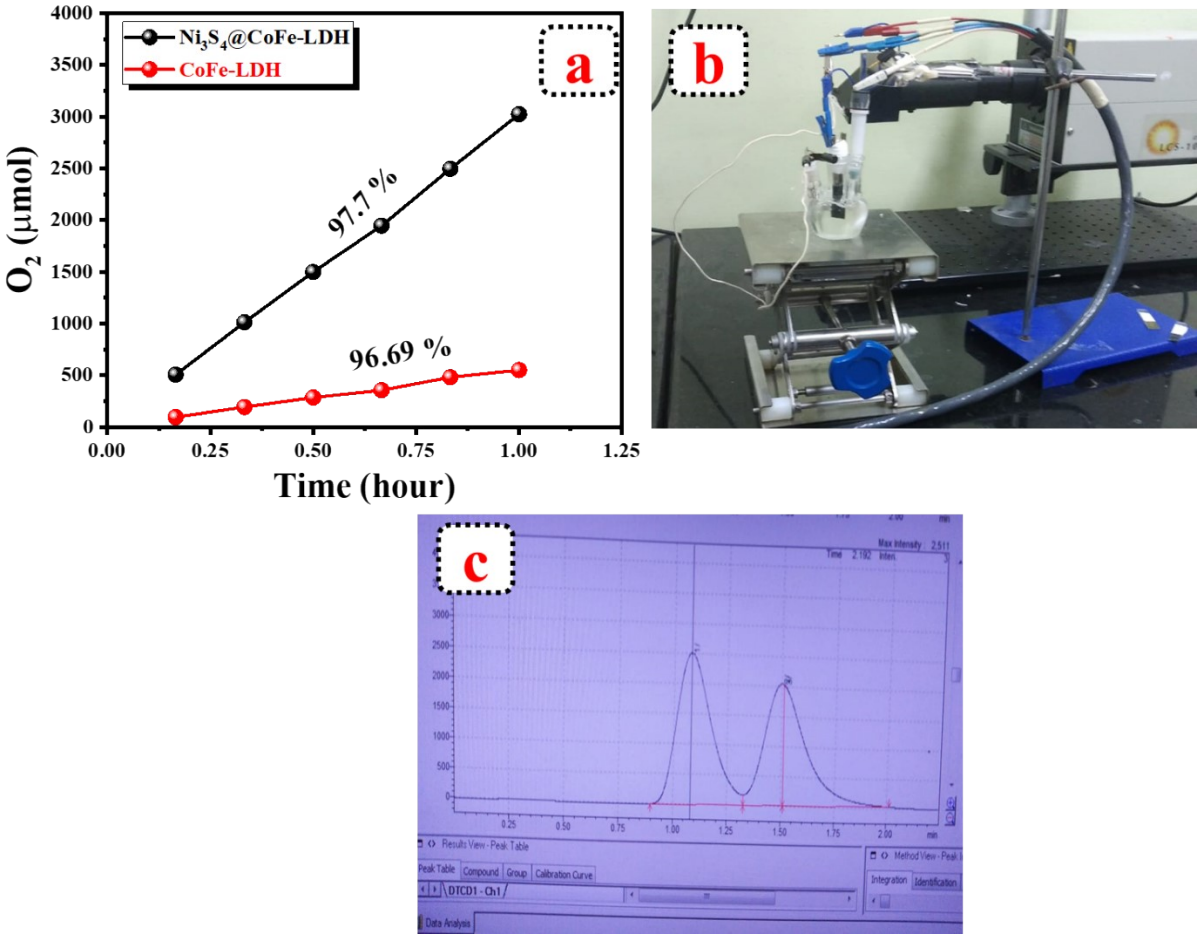

Figure S13. (a) Faradaic efficiency plot for CoFe-LDH and Ni_3S_4@CoFe-LDH by comparing the measured and theoretically evolve gas through GC-MS; (b) Experimental set-up for chronoamperometric study to quantify the evolve gas and (c) Typical GC-MS features for Ni_3S_4@CoFe-LDH.

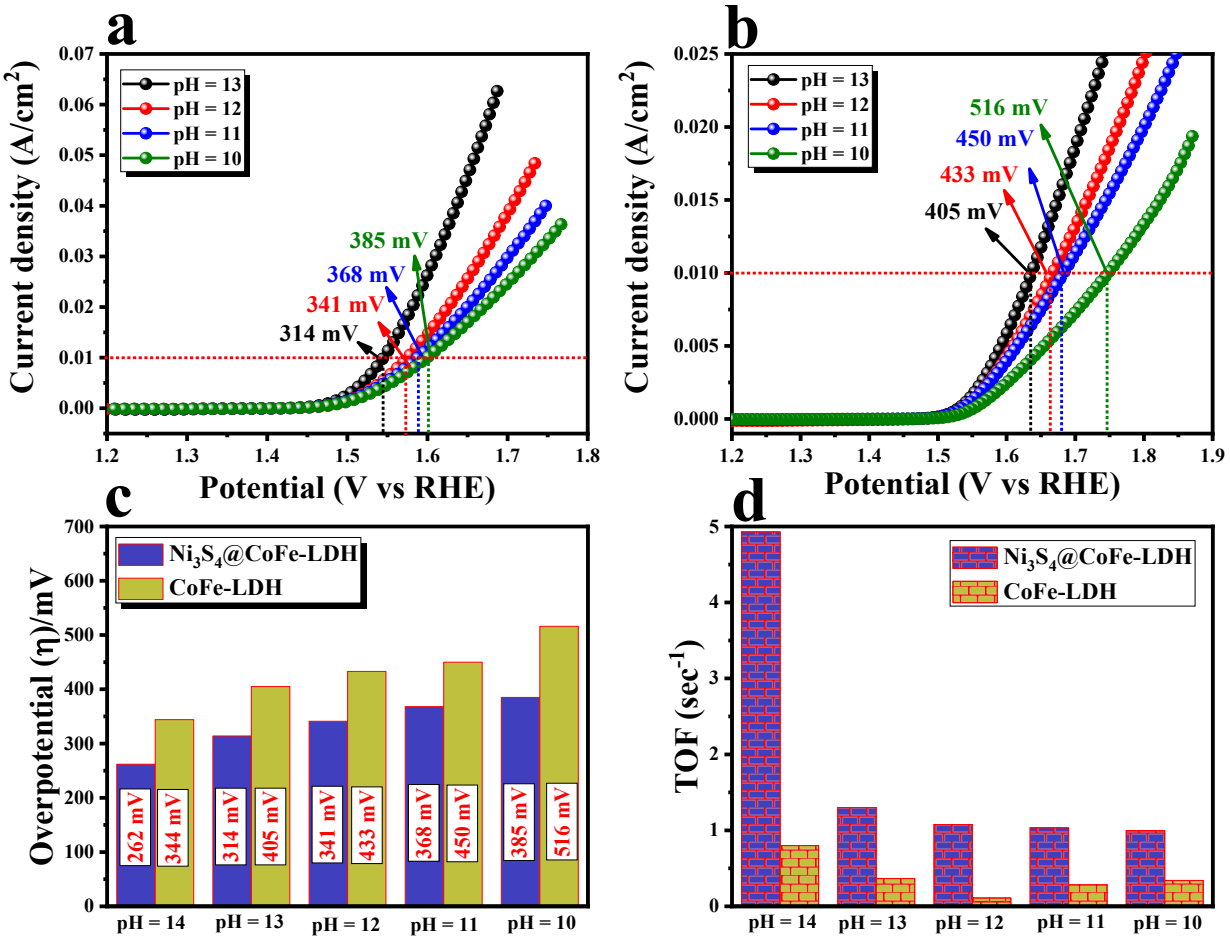

Figure S14. (a) LSV polarization outcomes of Ni_3S_4@CoFe-LDH at different pH value of 13, 12, 11 and 10; (b) LSV polarization outcomes of CoFe-LDH at different pH value of 13, 12, 11 and 10; (c) Comparison of overpotential data of Ni_3S_4@CoFe-LDH and CoFe-LDH and (d) Calculated TOF values for Ni3S4@CoFe-LDH at different pH condition.

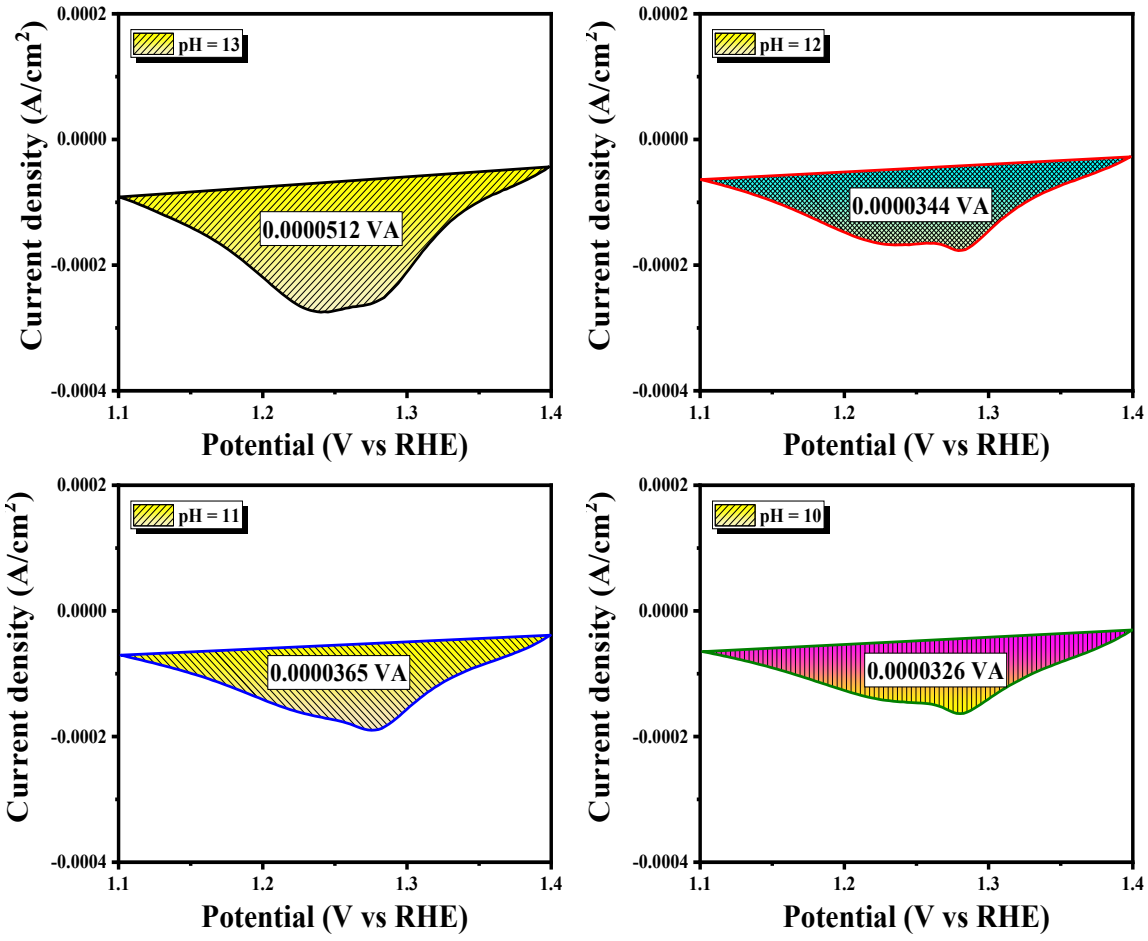

Figure S15. Reduction surface area of Ni_3S_4@CoFe-LDH at different pH values.

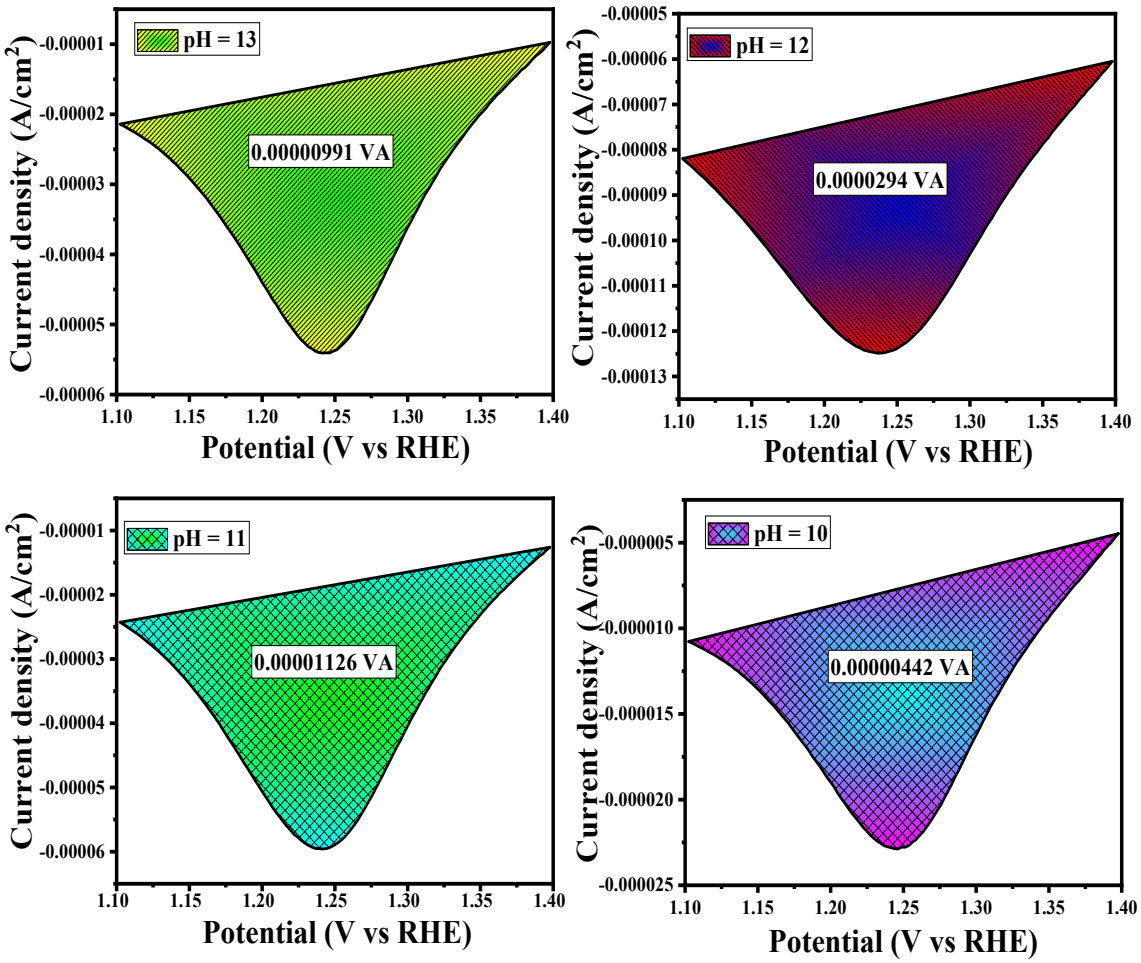

Figure S16. Reduction surface area of CoFe-LDH at different pH values.

Serial No.	Materials	Overpotential (mV)@ 10 mA/cm^2	Tafel Slope (mV/dec)	TOF (sec^{-1})	Ref.
1	CoNx@GDY NS/NF	260	84	-	1
2	MoS_2/Ni_3S_2	218	88	-	2
3	$NiCo_2S_4$@NiFe-LDH	201 mV	46.3	-	3
4	Co_9S_8-$CoSe_2$	340	96	2.25	4
5	CoNi hydroxide@hydroxysulfide	274	45	-	5
6	NiFe LDH@NiCoP/NF	220	48.6	-	6
7	Mo-Ni_3S_2/Ni_xP_y	238	60.6	-	7
8	$Ir/Ni(OH)_2$	224	41	~4	8
9	Co_9S_8@Co_9S_8@MoS_2-0.5	340	71.5	-	9
10	NiFeS/CoS	170	54.7	0.32	10
11	CoP/CeO_2	224	90.3	-	11
12	RuO_2/CeO_2	350	74	-	12
13	Ni_3S_2@NiV-LDH	190	57	-	13
14	CoP/TiO_x	337	72.1	-	14
15	Mo-$NiCo_2O_4/Co_{5.47}N$/NF	~300	55.1	-	15
16	CoFe LDH/$Co_{0.85}Se$	241	48	0.0439	16
17	CoFe-LDH/MXene	319	50	-	17
19	**Ni_3S_4@CoFe-LDH**	**262**	**70.2**	**4.93**	**This work**

Table S2. Comparison of electrochemical data of Ni_3S_4@CoFe-LDH with similar types of catalyst reported recently.

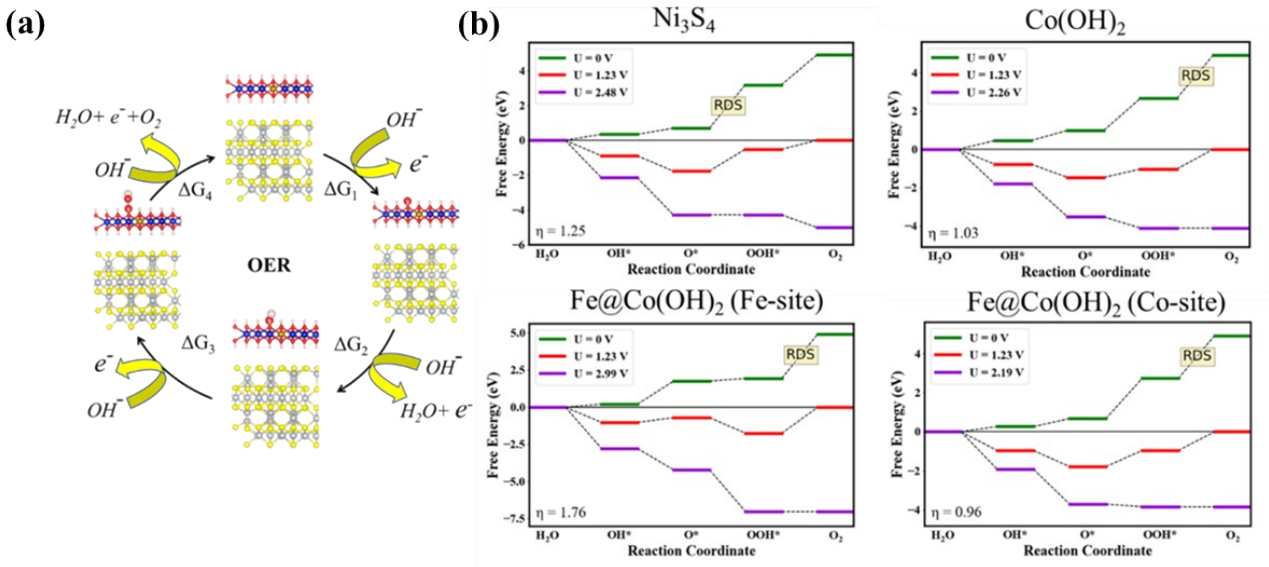

Figure S17. (a) Schematic representation of OER mechanism on CoFe-LDH/Ni_3S_4. (b)The calculated Gibbs free energy reaction profile of Ni_3S_4, $Co(OH)_2$, CoFe-LDH (Fe-site), and CoFe-LDH (Co-site) individual layer plot is shown.

References:

1 Y. Fang, Y. Xue, L. Hui, H. Yu, Y. Liu, C. Xing, F. Lu, F. He, H. Liu and Y. Li, *Nano Energy*, 2019, **59**, 591–597.

2 J. Zhang, T. Wang, D. Pohl, B. Rellinghaus, R. Dong and S. Liu, .

3 J. Liu, J. Wang, B. Zhang, Y. Ruan, L. Lv, X. Ji, K. Xu, L. Miao and J. Jiang, *ACS Appl. Mater. Interfaces*, 2017, **9**, 15364–15372.

4 S. Chakrabartty, S. Karmakar and C. R. Raj, *ACS Appl. Nano Mater.*, 2020, **3**, 11326–11334.

5 B. Wang, C. Tang, H. F. Wang, X. Chen, R. Cao and Q. Zhang, *Adv. Mater.*, 2019, **31**, 1–7.

6 H. Zhang, X. Li, A. Hähnel, V. Naumann, C. Lin, S. Azimi, S. L. Schweizer, A. W. Maijenburg and R. B. Wehrspohn, *Adv. Funct. Mater.*, 2018, **28**, 1–10.

7 X. Luo, P. Ji, P. Wang, R. Cheng, D. Chen, C. Lin, J. Zhang, J. He, Z. Shi, N. Li, S. Xiao and S. Mu, *Adv. Energy Mater.*, 2020, **10**, 1–11.

8 G. Zhao, P. Li, N. Cheng, S. X. Dou and W. Sun, *Adv. Mater.*, 2020, **32**, 1–9.

9 J. Li, G. Li, J. Wang, C. Xue, X. Li, S. Wang, B. Han, M. Yang and L. Li, *Inorg. Chem. Front.*, 2019, **7**, 191–197.

10 J. Tang, X. Jiang, L. Tang, Y. Li, Q. Zheng, Y. Huo and D. Lin, *Dalt. Trans.*, 2021, **50**, 5921–5930.

11 M. Li, X. Pan, M. Jiang, Y. Zhang, Y. Tang and G. Fu, *Chem. Eng. J.*, 2020, **395**, 125160.

12 S. M. Galani, A. Mondal, D. N. Srivastava and A. B. Panda, *Int. J. Hydrogen Energy*, 2020, **45**, 18635–18644.

13 Q. Liu, J. Huang, Y. Zhao, L. Cao, K. Li, N. Zhang, D. Yang, L. Feng and L. Feng, *Nanoscale*, 2019, **11**, 8855–8863.

14 Z. Liang, W. Zhou, S. Gao, R. Zhao, H. Zhang, Y. Tang, J. Cheng, T. Qiu, B. Zhu, C. Qu, W. Guo, Q. Wang and R. Zou, *Small*, 2020, **16**, 1–10.

15 W. Liu, L. Yu, R. Yin, X. Xu, J. Feng, X. Jiang, D. Zheng, X. Gao, X. Gao, W. Que, P. Ruan, F. Wu, W. Shi and X. Cao, *Small*, 2020, **16**, 1–8.

16 W. Jin, F. Liu, X. Guo, J. Zhang, L. Zheng, Y. Hu, J. Mao, H. Liu, Y. Xue and C. Tang, *Catal. Sci. Technol.*, 2019, **9**, 5736–5744.

17 C. Hao, Y. Wu, Y. An, B. Cui, J. Lin, X. Li, D. Wang, M. Jiang, Z. Cheng and S. Hu, *Mater. Today Energy*, 2019, **12**, 453–462.